

# OCT-GAN: Neural ODE-based Conditional Tabular GANs

Jayoung Kim, Jinsung Jeon, Jaehoon Lee, Jihyeon Hyeong, Noseong Park

{jayoung.kim,jjsjjs0902,ljh5694,jiji.hyeong,noseong}@yonsei.ac.kr

Yonsei University

Seoul, South Korea

## ABSTRACT

Synthesizing tabular data is attracting much attention these days for various purposes. With sophisticate synthetic data, for instance, one can augment its training data. For the past couple of years, tabular data synthesis techniques have been greatly improved. Recent work made progress to address many problems in synthesizing tabular data, such as the imbalanced distribution and multimodality problems. However, the data utility of state-of-the-art methods is not satisfactory yet. In this work, we significantly improve the utility by designing our generator and discriminator based on neural ordinary differential equations (NODEs). After showing that NODEs have theoretically preferred characteristics for generating tabular data, we introduce our designs. The NODE-based discriminator performs a hidden vector evolution trajectory-based classification rather than classifying with a hidden vector at the last layer only. Our generator also adopts an ODE layer at the very beginning of its architecture to transform its initial input vector (i.e., the concatenation of a noisy vector and a condition vector in our case) onto another latent vector space suitable for the generation process. We conduct experiments with 13 datasets, including but not limited to insurance fraud detection, online news article prediction, and so on, and our presented method outperforms other state-of-the-art tabular data synthesis methods in many cases of our classification, regression, and clustering experiments.

## CCS CONCEPTS

• Computing methodologies → Machine learning; Neural networks.

## KEYWORDS

Tabular Data Synthesis, Generative Adversarial Networks, Neural Ordinary Differential Equations

## ACM Reference Format:

Jayoung Kim, Jinsung Jeon, Jaehoon Lee, Jihyeon Hyeong, Noseong Park. 2021. OCT-GAN: Neural ODE-based Conditional Tabular GANs. In *Proceedings of the Web Conference 2021 (WWW '21)*, April 19–23, 2021, Ljubljana, Slovenia. ACM, New York, NY, USA, 10 pages. <https://doi.org/10.1145/3442381.3449999>

## 1 INTRODUCTION

Many web-based applications use tabular data and many enterprise systems use relational database management systems [53]. For these

This paper is published under the Creative Commons Attribution 4.0 International (CC-BY 4.0) license. Authors reserve their rights to disseminate the work on their personal and corporate Web sites with the appropriate attribution.

WWW '21, April 19–23, 2021, Ljubljana, Slovenia

© 2021 IW3C2 (International World Wide Web Conference Committee), published under Creative Commons CC-BY 4.0 License.

ACM ISBN 978-1-4503-8312-7/21/04.

<https://doi.org/10.1145/3442381.3449999>

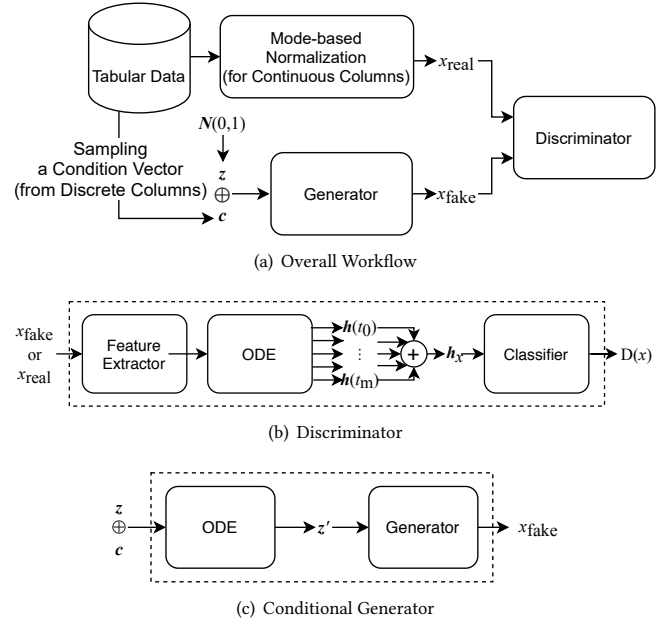


**Figure 1: Our proposed OCT-GAN architecture. (a) We preprocess raw tabular data with a mode-based normalization technique (See Section 3.1). (b) The discriminator adopts an ODE layer to perform a trajectory-based classification (See Section 3.2). (c) The ODE layer in the generator transforms  $z \oplus c$ , the concatenation of a noisy vector  $z$  and a condition vector  $c$ , into another latent vector  $z'$  that will be fed into the generator (See Section 3.3).**

reasons, many web-oriented researchers focus on various tasks on tabular data [10, 12, 27, 30, 32, 45, 56, 59, 62, 63]. In this work, generating realistic synthetic tabular data is of our utmost interest. If the utility of synthetic data is reasonably high while being different enough from real data, it can greatly benefit many applications by enabling to use the synthetic data as (additional) training data [2, 3, 11, 14, 17, 23, 40, 55]. In one of our experiments, for instance, we synthesize a feature table extracted from raw online news articles to predict the number of shares (e.g., tweets and retweets) in social networks.

Generative adversarial networks (GANs), which consist of a generator and a discriminator, are one of the most successful generative models [1, 4, 29, 31, 50]. GANs have been extended to various domains, ranging from images and texts to tables. Recently, Xu et al. introduced a tabular GAN, called TGAN, to synthesize tabular data [57]. TGAN now shows the state-of-the-art performance among existing GANs in generating tables in terms of *model compatibility*,

i.e., a machine learning model trained with synthetic (generated) data shows reasonable accuracy for unknown real test cases. In some cases, however, it is outperformed by non-GAN-based methods.

As noted in [13, 16, 42, 57], tabular data has irregular distribution and multimodality in many cases and existing techniques do not work. Based on the recent seminal work introducing Neural ODEs (NODEs) [21, 28, 46, 64], to this end, we design a novel NODE-based conditional tabular GAN, called OCT-GAN. Fig. 1 shows its detail design. In NODEs, a neural network  $f$  learns a system of ordinary differential equations to approximate  $\frac{dh(t)}{dt}$ , where  $\mathbf{h}(t)$  is a hidden vector at time (or layer)  $t$ . Given a sample  $x$  (i.e., a row or record in a table in our context), therefore, we can easily extract its hidden vector evolution trajectory from  $t_0$  to  $t_m$  while solving an integral problem, i.e.,  $\mathbf{h}(t_m) = \mathbf{h}(t_0) + \int_{t_0}^{t_m} f(\mathbf{h}(t), t; \theta_f) dt$ , where  $\theta_f$  means a set of parameters to learn for  $f$ . NODEs convert the integral problem into multiple steps of additions and we can retrieve a trajectory from those steps, i.e.,  $\{\mathbf{h}(t_0), \mathbf{h}(t_1), \mathbf{h}(t_2), \dots, \mathbf{h}(t_m)\}$ . Our discriminator equipped with a learnable ODE utilizes the extracted evolution trajectory to distinguish between real and synthetic samples (whereas other neural networks use only the last hidden vector, e.g.,  $\mathbf{h}(t_m)$  in the above example). This trajectory-based classification brings non-trivial freedom to the discriminator, making it be able to provide better feedback to the generator. Additional key part in our design is how to decide those time points  $t_i$ , for all  $i$ , to extract trajectories. We let the model learn them from data.

NODEs have one more characteristic in favor of our generator as well. That is, NODEs can be seen as a mapping function from  $t_0$  to  $t_m$  and the mapping function is always homeomorphic, i.e., bijective and continuous. We use this homeomorphic mapping to transform the initial input of our conditional generator, i.e., a noisy vector concatenated with a condition vector, into a latent vector in another vector space suitable for remaining procedures in the generator. A homeomorphic mapping does not drastically change input and the topology of input space is maintained in its output space. Therefore, we can maintain the original semantics of the noisy and condition vectors while mapping to another latent vector. One additional advantage of adopting a homeomorphic mapping is that it enables us to achieve smooth interpolations of generated fake samples.

We conduct experiments with 13 datasets for various machine learning tasks. Among all tested baseline methods to synthesize tabular data, the proposed OCT-GAN shows the best performance for many cases of our classification, regression, and clustering experiments. In addition, our method shows smooth interpolations of noisy vectors. Our contributions can be summarized as follows:

- (1) Our discriminator has an ODE layer to extract a hidden vector evolution trajectory for classification.
- (2) The trajectory is represented by a series of hidden vectors extracted at various layers (or time)  $t_i$ . We also train these extraction time points.
- (3) The trajectory-based classification brings non-trivial benefits to the discriminator since we can use not only the last hidden vector but also all the information contained in the trajectory.
- (4) Our generator adopts an initial ODE layer to transform  $\mathbf{z} \oplus \mathbf{c}$  to another latent hidden vector  $\mathbf{z}'$  suitable for the generation

process (while maintaining the semantics contained in  $\mathbf{z} \oplus \mathbf{c}$ , i.e., a homeomorphic mapping).

- (5) We conduct in-depth experiments with 13 datasets in total, ranging from insurance fraud detection to online news article spread prediction and so on. Our evaluation tasks include generating fake tabular data for likelihood estimation, classification, regression, and clustering, and our method outperforms existing methods by large margins in many cases.

## 2 RELATED WORK

We review the literature related to our work. We first introduce recent progress on GANs and then various tabular data synthesis techniques. We also describe NODEs in detail.

### 2.1 Generative Adversarial Networks

GANs consist of two neural networks: a generator and a discriminator. They perform a two-play zero-sum game and its equilibrium state is theoretically well defined, where the generator achieves the optimal generation quality and the discriminator cannot distinguish between real and fake samples. WGAN and its variants are widely used among many GANs proposed so far [1, 4, 31]. In particular, WGAN-GP is one of the most successful models and is defined as follows:

$$\min_G \max_D \mathbb{E}[D(\mathbf{x})]_{\mathbf{x} \sim p_{\mathbf{x}}} - \mathbb{E}[D(G(\mathbf{z}))]_{\mathbf{z} \sim p_{\mathbf{z}}} - \lambda \mathbb{E}[(\|\nabla_{\bar{\mathbf{x}}} D(\bar{\mathbf{x}})\|_2 - 1)^2]_{\bar{\mathbf{x}} \sim p_{\bar{\mathbf{x}}}}, \quad (1)$$

where  $p_{\mathbf{z}}$  is a prior distribution;  $p_{\mathbf{x}}$  is a distribution of data;  $G$  is a generator function;  $D$  is a discriminator (or Wasserstein critic) function;  $\bar{\mathbf{x}}$  is a randomly weighted combination of  $G(\mathbf{z})$  and  $\mathbf{x}$ . The discriminator provides feedback on the quality of the generation. In addition, we let  $p_g$  be a distribution of fake data induced by the function  $G(\mathbf{z})$  from  $p_{\mathbf{z}}$ , and  $p_{\bar{\mathbf{x}}}$  be a distribution created after the random combination. We typically use  $\mathcal{N}(0, 1)$  for the prior  $p_{\mathbf{z}}$ . Many task-specific GAN models are designed on top of the WGAN-GP framework. We use  $\mathcal{L}_D$ ,  $\mathcal{L}_G$  to denote the WGAN-GP's loss functions to train the discriminator and the generator, respectively.

A popular variant of GANs are conditional GANs [34, 39]. Under the regime of conditional GANs, the generator  $G(\mathbf{z}, \mathbf{c})$  is fed with a noisy vector  $\mathbf{z}$  and a condition vector  $\mathbf{c}$ . In many cases, the condition vector is a one-hot vector denoting a class label to generate.

### 2.2 Tabular Data Synthesis

Tabular data synthesis, which generates a realistic synthetic table by modeling a joint probability distribution of columns in a table, encompasses many different methods depending on the types of data. For instance, Bayesian networks [6, 60] and decision trees [48] are used to generate discrete variables. A recursive modeling of tables using the Gaussian copula is used to generate continuous variables [44]. A differentially private algorithm for decomposition is used to synthesize spatial data [19, 61]. However, some constraints that these models have such as the type of distributions and computational problems have hampered high-fidelity data synthesis.

In recent years, several data generation methods based on GANs have been introduced to synthesize tabular data, which mostly handle healthcare records. RGAN [25] generates continuous time-series healthcare records while MedGAN [16], corrGAN [43] generate

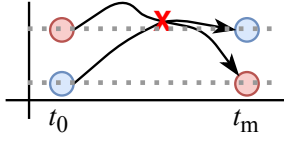


**Figure 2: The locations of the red and blue points are swapped by the mapping from  $t_0$  to  $t_m$ . NODEs cannot simultaneously learn the red and blue trajectories that cross each other since their topology (i.e., their relative positions) cannot be changed after a mapping in NODEs.**

discrete records. EhrGAN [13] generates plausible labeled records using semi-supervised learning to augment limited training data. PATE-GAN [35] generates synthetic data without endangering the privacy of original data. TableGAN [42] improved tabular data synthesis using convolutional neural networks to maximize the prediction accuracy on the label column.

### 2.3 Neural Ordinary Differential Equations

Let  $\mathbf{h}(t)$  be a function that outputs a hidden vector at time (or layer)  $t$  in a neural network. In Neural ODEs (NODEs), a neural network  $f$  with a set of parameters, denoted  $\theta_f$ , approximates  $\frac{d\mathbf{h}(t)}{dt}$ , and  $\mathbf{h}(t_m)$  is calculated by  $\mathbf{h}(t_0) + \int_{t_0}^{t_m} f(\mathbf{h}(t), t; \theta_f) dt$ , where  $f(\mathbf{h}(t), t; \theta_f) = \frac{d\mathbf{h}(t)}{dt}$ . In other words, the internal dynamics of the hidden vector evolution process is described by a system of ODEs parameterized by  $\theta_f$ . One advantage of using NODEs is that we can interpret  $t$  as continuous, which is discrete in usual neural networks. Therefore, more flexible constructions are possible in NODEs, which is one of the main reasons why we adopt an ODE layer in our discriminator.

To solve the integral problem,  $\mathbf{h}(t_0) + \int_{t_0}^{t_m} f(\mathbf{h}(t), t; \theta_f) dt$ , in NODEs, we rely on an ODE solver which transforms an integral into a series of additions. The Dormand–Prince (DOPRI) method [22] is one of the most powerful integrators and is widely used in NODEs. It is a member of the Runge–Kutta family of ODE solvers. DOPRI dynamically controls its step size while solving an integral problem. It is now the default method in MATLAB, GNU Octave, etc.

Let  $\phi_t : \mathbb{R}^{\dim(\mathbf{h}(t_0))} \rightarrow \mathbb{R}^{\dim(\mathbf{h}(t_m))}$  be a mapping from  $t_0$  to  $t_m$  created by an ODE after solving the integral problem. It is well-known that  $\phi_t$  becomes a homeomorphic mapping:  $\phi_t$  is continuous and bijective and  $\phi_t^{-1}$  is also continuous for all  $t \in [0, T]$ , where  $T$  is the last time point of the time domain [24, 38]. From this characteristic, the following proposition can be derived:

**PROPOSITION 2.1.** *The topology of the input space of  $\phi_t$  is preserved in its output space, and therefore, trajectories crossing each other cannot be represented by NODEs, e.g., Fig. 2.*

While preserving the topology, NODEs can perform machine learning tasks and it was shown in [58] that it increases the robustness of representation learning to adversarial attacks.

Instead of the backpropagation method, the adjoint sensitivity method is used to train NODEs for its efficiency and theoretical correctness [15]. After letting  $\mathbf{a}_h(t) = \frac{d\mathcal{L}}{d\mathbf{h}(t)}$  for a task-specific loss  $\mathcal{L}$ , it calculates the gradient of loss w.r.t model parameters with

another reverse-mode integral as follows:

$$\nabla_{\theta_f} \mathcal{L} = \frac{d\mathcal{L}}{d\theta_f} = - \int_{t_m}^{t_0} \mathbf{a}_h(t)^\top \frac{\partial f(\mathbf{h}(t), t; \theta_f)}{\partial \theta_f} dt.$$

$\nabla_{\mathbf{h}(0)} \mathcal{L}$  can also be calculated in a similar way and we can propagate the gradient backward to layers earlier than the ODE if any. It is worth mentioning that the space complexity of the adjoint sensitivity method is  $O(1)$  whereas using the backpropagation to train NODEs has a space complexity proportional to the number of DOPRI steps. Their time complexities are similar or the adjoint sensitivity method is slightly more efficient than that of the backpropagation. Therefore, we can train NODEs efficiently.

## 3 PROPOSED METHODS

In this section, we describe our OCT-GAN. We first describe our data preprocessing method, and then describe both our discriminator and generator. We adopt an ODE layer for the following reasons in each of the discriminator and the generator:

- (1) In the discriminator, we can interpret time (or layer)  $t$  as continuous in its ODE layer. We can also perform trajectory-based classification by finding optimal time points that lead to improved classification performance.
- (2) In the conditional generator, we exploit the homeomorphic characteristic of NODEs to transform  $\mathbf{z} \oplus \mathbf{c}$  onto another latent space while preserving the (semantic) topology of the initial latent space. We propose to use this because i) a data distribution in tabular data is irregular and difficult to directly capture [57] and ii) by finding an appropriate latent space the generator can generate better samples [36]. At the same time, interpolating noisy vectors given a fixed condition can be smooth.
- (3) Therefore, the entire generation process can be separated into the following two stages as in Fig. 5: 1) transforming the initial input space into another latent space (potentially close to a real data distribution) while maintaining the topology of the input space, and 2) the remaining generation process finds a fake distribution matched to the real data distribution.

### 3.1 Preprocessing of Tabular Data

We consider tabular data with two types of columns: discrete columns, denoted  $\{D_1, D_2, \dots, D_{N_D}\}$ , and continuous columns, denoted  $\{C_1, C_2, \dots, C_{N_C}\}$ . Discrete values are transformed to one-hot vectors as usual. However, continuous values are preprocessed with a mode-specific normalization technique [57]. GANs generating tabular data frequently suffer from mode collapse and irregular data distribution. By specifying modes before training, the mode-specific normalization can alleviate the problems. The  $i_{th}$  raw sample  $r_i$  (a row or record in the tabular data) can be written as  $d_{i,1} \oplus d_{i,2} \oplus \dots \oplus d_{i,N_D} \oplus c_{i,1} \oplus c_{i,2} \oplus \dots \oplus c_{i,N_C}$ , where  $d_{i,j}$  (resp.  $c_{i,j}$ ) is a value in column  $D_j$  (resp. column  $C_j$ ). After the following three steps, the raw sample  $r_i$  is preprocessed to  $x_i$ .

- (1) Each discrete values  $\{d_{i,1}, d_{i,2}, \dots, d_{i,N_D}\}$  are transformed to one-hot vector  $\{\mathbf{d}_{i,1}, \mathbf{d}_{i,2}, \dots, \mathbf{d}_{i,N_D}\}$ .
- (2) Using the variational Gaussian mixture (VGM) model, we fit each continuous column  $C_j$  to a Gaussian mixture. The fitted Gaussian mixture is  $\Pr_j(c_{i,j}) = \sum_{k=1}^{n_j} w_{j,k} \mathcal{N}(c_{i,j}; \mu_{j,k}, \sigma_{j,k})$ ,

where  $n_j$  is the number of modes (i.e., the number of Gaussian distributions) in columns  $C_j$ .  $w_{j,k}$ ,  $\mu_{j,k}$ ,  $\sigma_{j,k}$  are a fitted weight, mean and standard deviation of  $k_{th}$  Gaussian distribution.

- (3) With a probability of  $\Pr_j(k) = \frac{w_{j,k} \mathcal{N}(c_{i,j}; \mu_{j,k}, \sigma_{j,k})}{\sum_{p=1}^{n_j} w_{j,p} \mathcal{N}(c_{i,j}; \mu_{j,p}, \sigma_{j,p})}$ , we sample an appropriate mode  $k$  for  $c_{i,j}$ . We then normalize  $c_{i,j}$  from the mode  $k$  with its fitted standard deviation, and save the normalized value  $\alpha_{i,j}$  and the mode information  $\beta_{i,j}$ . For example, if there are 4 modes and we pick the third mode, i.e.,  $k = 3$ , then  $\alpha_{i,j}$  is  $\frac{c_{i,j} - \mu_3}{4\sigma_3}$  and  $\beta_{i,j}$  is  $[0, 0, 1, 0]$ .
- (4) As a result,  $r_i$  is transformed to  $x_i$  which is denoted as follows:

$$x_i = \alpha_{i,1} \oplus \beta_{i,1} \oplus \dots \oplus \alpha_{i,N_c} \oplus \beta_{i,N_c} \oplus \mathbf{d}_{i,1} \oplus \dots \oplus \mathbf{d}_{i,N_D}.$$

We note that in  $x_i$ , we can specify the detailed mode-based information of  $r_i$ . Our discriminator and generator work with  $x_i$  instead of  $r_i$  for its clarification on modes. However,  $x_i$  can be readily changed to  $r_i$ , once generated, using the fitted parameters of the Gaussian mixture.

### 3.2 Discriminator

We design a NODE-based discriminator and consider the trajectory of  $\mathbf{h}(t)$ , where  $t \in [0, t_m]$ , when predicting whether an input sample  $x$  is real or fake. To this end, we use the following ODE-based discriminator that outputs  $D(x)$  given a (preprocessed or generated) sample  $x$ :

$$\mathbf{h}(0) = \text{Drop}(\text{Leaky}(\text{FC2}(\text{Drop}(\text{Leaky}(\text{FC1}(x)))))), \quad (2)$$

$$\mathbf{h}(t_1) = \mathbf{h}(0) + \int_0^{t_1} f(\mathbf{h}(0), t; \theta_f) dt, \quad (3)$$

$$\mathbf{h}(t_2) = \mathbf{h}(t_1) + \int_{t_1}^{t_2} f(\mathbf{h}(t_1), t; \theta_f) dt, \quad (4)$$

$$\vdots \quad (5)$$

$$\mathbf{h}(t_m) = \mathbf{h}(t_{m-1}) + \int_{t_{m-1}}^{t_m} f(\mathbf{h}(t_{m-1}), t; \theta_f) dt, \quad (6)$$

$$\mathbf{h}_x = \mathbf{h}(0) \oplus \mathbf{h}(t_1) \oplus \mathbf{h}(t_2) \oplus \dots \oplus \mathbf{h}(t_m), \quad (7)$$

$$D(x) = \text{FC5}(\text{Leaky}(\text{FC4}(\text{Leaky}(\text{FC3}(\mathbf{h}_x))))), \quad (8)$$

where  $\oplus$  means the concatenation operator, Leaky is the leaky ReLU, Drop is the dropout, and FC is the fully connected layer. The ODE function  $f(\mathbf{h}(t), t; \theta_f)$  is defined as follows:

$$\text{ReLU}(\text{BN}(\text{FC7}(\text{ReLU}(\text{BN}(\text{FC6}(\text{ReLU}(\text{BN}(\mathbf{h}(t))) \oplus t))))), \quad (9)$$

where BN is the batch normalization and ReLU is the rectified linear unit.

We note that the trajectory of  $\mathbf{h}(t)$  is continuous in NODEs. However, it is difficult to consider continuous trajectories in training GANs. To discretize the trajectory of  $\mathbf{h}(t)$ , therefore,  $t_1, t_2, \dots, t_m$  are trained and  $m$  is a hyperparameter in our proposed method. We also note that Eqs. (3) to (6) share the same parameter  $\theta_f$ , which means they constitute a single system of ODEs but for the purpose of discretization we separate them. After letting  $\mathbf{a}_t(t) = \frac{d\mathcal{L}}{dt}$ , we use the following gradient definition (derived from the adjoint sensitivity method) to train  $t_i$  for all  $i$ :

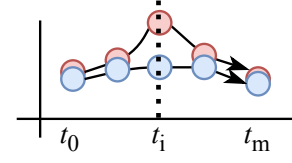


**Figure 3:** Suppose that the two red/blue trajectories from  $t_0$  to  $t_m$  are all similar except around  $t_i$ . Because we train such distinguishing time points, our trajectory-based classification can correctly classify them. Without training  $t_i$ , those intermediate time points should be set by user, which is sub-optimal.

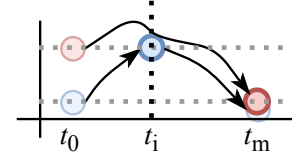


**Figure 4:** The red and blue trajectories do not cross each other and can be learned by NODEs. By taking the blue hidden vector at  $t_i$  and the red hidden vector at  $t_m$ , however, we can swap their positions, which is impossible in Fig. 2. Therefore, our trajectory-based classification is necessary to improve NODEs.

**PROPOSITION 3.1.** The gradient of loss  $\mathcal{L}$  w.r.t.  $t_m$  can be calculated in the following way:

$$\nabla_{t_m} \mathcal{L} = \frac{d\mathcal{L}}{dt_m} = \mathbf{a}_h(t_m) f(\mathbf{h}(t_m), t_m; \theta_f).$$

**PROOF.** First, because  $\mathbf{a}_h(t_m) = \frac{d\mathcal{L}}{d\mathbf{h}(t_m)}$  by its definition,

$$\mathbf{a}_h(t_m) f(\mathbf{h}(t_m), t_m; \theta_f) = \frac{d\mathcal{L}}{d\mathbf{h}(t_m)} f(\mathbf{h}(t_m), t_m; \theta_f),$$

and then by the definition of  $f$ ,

$$\frac{d\mathcal{L}}{d\mathbf{h}(t_m)} f(\mathbf{h}(t_m), t_m; \theta_f) = \frac{d\mathcal{L}}{d\mathbf{h}(t_m)} \frac{d\mathbf{h}(t_m)}{dt_m} = \frac{d\mathcal{L}}{dt_m}.$$

□

For the same reason above,  $\nabla_{t_i} \mathcal{L} = \frac{d\mathcal{L}}{dt_i} = \mathbf{a}_h(t_i) f(\mathbf{h}(t_i), t_i; \theta_f)$  where  $i < m$ . But we do not want to save any intermediate adjoint states for space complexity purposes and calculate the gradient with a reverse-mode integral as follows:

$$\nabla_{t_i} \mathcal{L} = \mathbf{a}_h(t_m) f(\mathbf{h}(t_m), t_m; \theta_f) - \int_{t_m}^{t_i} \mathbf{a}_h(t) \frac{\partial f(\mathbf{h}(t), t; \theta_f)}{\partial t} dt.$$

We note that we need to save only one adjoint state  $\mathbf{a}_h(t_m)$  and calculate  $\nabla_{t_i} \mathcal{L}$  with the two functions  $f$  and  $\mathbf{a}_h(t)$ .

We typically use the last hidden vector  $\mathbf{h}(t_m)$  for classification. In our case, however, we use the entire trajectory for classification. When using only the last hidden vector, all needed information for classification should be correctly captured in it. In our setting, however, even two similar last hidden vectors can be easily distinguished if their intermediate trajectories are different at least at a value of  $t$ .

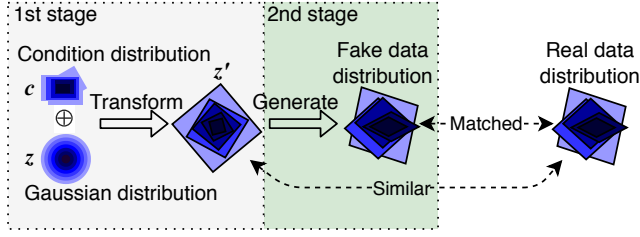


**Figure 5: The ODE layer in the generator transforms the concatenation of a noisy vector and a condition vector,  $z \oplus c$ , into  $z'$ . The 1st transformation is a homeomorphic mapping that maintains the original (semantic) topology whereas the 2nd generation process is not homeomorphic.**

In addition, we train  $t_i$ , which further improves the efficacy of the proposed method by finding key time points to distinguish trajectories. We note that training  $t_i$  is impossible in usual neural networks because their layer constructions are discrete. Fig. 3 illustrates such an example that only our NODE-based discriminator with learnable intermediate time points can correctly classify, and Fig. 4 also shows that our method can address the problem of the limited learning representation of NODEs.

### 3.3 Conditional Generator

The proposed OCT-GAN is a conditional GAN and its generator reads a noisy vector as well as a condition vector to generate a fake sample. Our definition of the condition vector is as follows:

$$c = c_1 \oplus \dots \oplus c_{N_D},$$

where  $c_i$  is either a zero vector or a random one-hot vector of the  $i_{th}$  discrete column. We randomly decide  $s \in \{1, 2, \dots, N_D\}$  and only  $c_s$  is a random one-hot vector and for all other  $i \neq s$ ,  $c_i$  is a zero vector, i.e., we specify a discrete value in the  $s_{th}$  discrete column.

Given an initial input  $\mathbf{p}(0) = z \oplus c$ , we feed it into an ODE layer to transform into another latent vector. We denote this transformed vector by  $z'$ . For this transformation, we use an ODE layer independent from the ODE layer in the discriminator as follows:

$$z' = \mathbf{p}(1) = \mathbf{p}(0) + \int_0^1 g(\mathbf{p}(t), t; \theta_g) dt.$$

We fix the integral time to  $[0, 1]$  because any ODE in  $[0, w]$ ,  $w > 0$ , with  $g$  can be reduced into a unit-time integral with  $g'$  by letting  $g' = \frac{g(\mathbf{p}(t), t; \theta_g)}{w}$ .

As noted earlier, an ODE is a homeomorphic mapping. We exploit the characteristic to design a semantically reliable mapping (or transformation). GANs typically use a noisy vector sampled from a Gaussian distribution, which is known as sub-optimal [36]. Thus, the transformation is needed in our case.

The Grönwall–Bellman inequality states that given an ODE  $\phi_t$  and its two initial states  $\mathbf{p}_1(0) = \mathbf{x}$  and  $\mathbf{p}_2(0) = \mathbf{x} + \delta$ , there exists a constant  $\tau$  such that  $\|\phi_t(\mathbf{x}) - \phi_t(\mathbf{x} + \delta)\| \leq \exp(\tau) \|\delta\|$  [41]. In other words, two similar input vectors with small  $\delta$  will be mapped to close to each other within a boundary of  $\exp(\tau) \|\delta\|$ .

In addition, we do not extract  $z'$  from intermediate time points so the generator’s ODE learns a homeomorphic mapping. Thus, the

topology of the initial input vector space is maintained. The initial input vector  $\mathbf{p}(0)$  contains non-trivial information on what to generate, e.g., condition, so we would like to maintain the relationships among initial input vectors while transforming them onto another latent vector space suitable for generation. Fig. 5 shows an example of our two-stage approach where i) the ODE layer finds a balancing distribution between the initial input distribution and the real data distribution and ii) the following procedures generate realistic fake samples. In particular, our transformation makes the interpolation of synthetic samples smooth, i.e., given two similar initial inputs, two similar synthetic samples are generated by the generator (as proved in the Grönwall–Bellman inequality) — we show these smooth interpolations in our experiment section. The proposed generator equipped with learning the optimal transformation is as follows:

$$\mathbf{p}(0) = z \oplus c, \quad (10)$$

$$z' = \mathbf{p}(0) + \int_0^1 g(\mathbf{p}(t), t; \theta_g) dt, \quad (11)$$

$$\mathbf{h}(0) = z' \oplus \text{ReLU}(\text{BN}(\text{FC1}(z'))), \quad (12)$$

$$\mathbf{h}(1) = \mathbf{h}(0) \oplus \text{ReLU}(\text{BN}(\text{FC2}(\mathbf{h}(0)))), \quad (13)$$

$$\hat{\alpha}_i = \text{Tanh}(\text{FC3}(\mathbf{h}(1))), 1 \leq i \leq N_c, \quad (14)$$

$$\hat{\beta}_i = \text{Gumbel}(\text{FC4}(\mathbf{h}(1))), 1 \leq i \leq N_c, \quad (15)$$

$$\hat{d}_j = \text{Gumbel}(\text{FC5}(\mathbf{h}(1))), 1 \leq j \leq N_d, \quad (16)$$

where  $\text{Tanh}$  is the hyperbolic tangent, and  $\text{Gumbel}$  is the Gumbel-softmax to generate one-hot vectors. The ODE function  $g(\mathbf{p}(t), t; \theta_g)$  is defined as follows:

$$\underbrace{\text{8 layers of FC and Leaky}}_{\text{Leaky}(\text{FC13}(\dots \text{Leaky}(\text{FC6}(\text{Norm}(\mathbf{p}(t)) \oplus t)) \dots))}, \quad (17)$$

where  $\text{Norm}(\mathbf{p}) = \frac{\mathbf{p}}{\|\mathbf{p}\|_2}$ .

As stated earlier, we specify a discrete value in a discrete column as a condition. Thus, it is required that  $\hat{d}_s = c_s$ , and we use a cross-entropy loss to enforce the match, denoted  $\mathcal{L}_{\text{matching}} = H(c_s, \hat{d}_s)$ . Another possible design choice is to copy  $c_s$  to  $\hat{d}_s$ . However, we do not copy for a principled training of the generator.

### 3.4 Training Algorithm

We train OCT-GAN using the loss in Eq. (1) in conjunction with  $\mathcal{L}_{\text{matching}}$  and its training algorithm is in Alg. 1. To train OCT-GAN, we need a real table  $T_{\text{train}}$ , and a maximum epoch number  $\text{max\_epoch}$ . After creating a mini-batch  $b$  (line 4), we perform the adversarial training (lines 5, 6), followed by updating  $t_i$  with the custom gradient calculated by the adjoint sensitivity method (line 7).

The space complexity to calculate  $\nabla_{t_i} \mathcal{L}$  is  $O(1)$  (see Section 3.2). Calculating  $\nabla_{t_j} \mathcal{L}$  subsumes the computation of  $\nabla_{t_i} \mathcal{L}$ , where  $t_0 \leq t_j < t_i \leq t_m$ . While solving the reverse-mode integral from  $t_m$  to  $t_0$ , thus, we can retrieve  $\frac{d\mathcal{L}}{dt_i}$  for all  $i$ . Therefore, the space complexity to calculate all the gradients is  $O(m)$  at line 7, which is additional overhead incurred by our method.

## 4 EXPERIMENTS

We describe our experimental environments and results for likelihood estimation, classification, regression, clustering, and so on.

**Algorithm 1:** How to train OCT-GAN

---

**Input** : A training table  $T_{\text{train}}$ ; a max epoch  $max\_epoch$ ;  
learning rates  $\lambda_G, \lambda_D, \lambda_t$

**Output** : A trained generator

- 1 Initialize a generator  $G$  and a discriminator  $D$
- 2  $k \leftarrow 0$
- 3 **while**  $k < max\_epoch$  **do**
- 4     **for each** mini-batch  $b \in T_{\text{train}}$  **do**
- 5         /\* Perform adversarial training. \*/
- 6         Train the discriminator  $D$  with mini-batch  $b$ , learning rate  $\lambda_D$ , and loss  $\mathcal{L}_D$
- 7         Train the generator  $G$  with mini-batch  $b$ , learning rate  $\lambda_G$ , loss  $\mathcal{L}_G + \mathcal{L}_{\text{matching}}$
- 8         /\* Update the intermediate time points. \*/
- 9          $t_i \leftarrow t_i - \lambda_t \nabla_{t_i} \mathcal{L}$ , for all  $i$
- 10      $k \leftarrow k + 1$
- 11     Anneal  $\lambda_G, \lambda_D, \lambda_t$  with a decay factor of  $\psi$  every  $\xi$  epoch
- 12 **return** the trained generator  $G$

---

## 4.1 Likelihood Estimation with Simulated Data

**4.1.1 Data.** We first conduct experiments with simulated datasets. We collected various pre-trained Bayesian networks and Gaussian mixture models from the literature. Using the pre-trained models (or oracles), we generate  $T_{\text{train}}$  and  $T_{\text{test}}$ , each of which is used for training and testing, respectively: Grid and Ring are from the Gaussian mixture models [54] and Alarm, Child, Asia, and Insurance are from the Bayesian networks [52] as summarized in Table 1.

**4.1.2 Evaluation Methodology.** One advantage of using the simulated data is that we can estimate the *likelihood fitness* of synthetic data given an oracle (pre-trained model)  $\mathcal{S}$ . The overall evaluation workflow is as follows:

- (1) Using  $T_{\text{train}}$ , we train generative models including OCT-GAN.
- (2) We generate synthetic data from each trained generative model. Let  $\mathcal{F}$  be this synthetic data.
- (3) We measure the likelihood of  $\mathcal{F}$  given  $\mathcal{S}$ , denoted  $\Pr(\mathcal{F}|\mathcal{S})$ .
- (4) We train another oracle  $\mathcal{S}'$  with  $\mathcal{F}$  from scratch.
- (5) We measure  $\Pr(T_{\text{test}}|\mathcal{S}')$ , the likelihood of  $T_{\text{test}}$  given  $\mathcal{S}'$ .

We note that the two likelihood estimates should be good enough at the same time. A low value for  $\Pr(T_{\text{test}}|\mathcal{S}')$  means that  $\mathcal{F}$  contains limited cases of  $T_{\text{train}}$ , i.e., mode collapse. We repeat the generation-testing experiments ten times to find their average performance, which is also the case in the remaining experiments in this paper.

**4.1.3 Baseline Methods.** We consider the following baselines: i) The case where we use  $T_{\text{train}}$  instead of  $\mathcal{F}$  is shown in the row titled “ $T_{\text{train}}$ ” in Tables 2 and 3; ii) CLBN [18] is a Bayesian network built by the Chow-Liu algorithm representing a joint probability distribution; iii) PrivBN [60] is a differentially private method for synthesizing tabular data using Bayesian networks; iv) MedGAN [16] is a GAN that generates discrete medical records by incorporating non-adversarial losses; v) VEEGAN [54] is a GAN that generates tabular data with an additional reconstructor network to avoid mode collapse; vi) TableGAN [42] is a GAN that generates tabular data using convolutional neural networks; vii) TVAE [33] is a variational

autoencoder (VAE) model to generate tabular data; viii) TGAN [57] is a GAN that generates tabular data with mixed types of variables. We use these baselines’ hyperparameters recommended in their original paper and github repositories.

**4.1.4 Hyperparameters.** We test the following sets of hyperparameters:  $\lambda_t = \lambda_G = \lambda_D = \{2e-3, 2e-4, 2e-5, 2e-6\}$ , the mini-batch size is  $\{500, 1000, 1500\}$ , and the number of intermediate time points to train in the discriminator is  $m = \{3, 5, 7\}$ . The maximum epoch number is  $max\_epoch = 300$ . The (input, output) dimensionality of each layer is as follows:

- (1) In the discriminator,
  - (a)  $(\dim(x), 256)$  for FC1,
  - (b)  $(256, 256)$  for FC2,
  - (c)  $(\dim(\mathbf{h}_x), 2 \dim(\mathbf{h}_x))$  for FC3,
  - (d)  $(2 \dim(\mathbf{h}_x), \dim(\mathbf{h}_x))$  for FC4,
  - (e)  $(\dim(\mathbf{h}_x), 1)$  for FC5,
  - (f)  $(\dim(\mathbf{h}(x)) + 1, \dim(\mathbf{h}(x)))$  for FC6,
  - (g)  $(\dim(\mathbf{h}(x)), \dim(\mathbf{h}(x)))$  for FC7.
- (2) In the generator,
  - (a)  $(\dim(\mathbf{p}(0)), 256)$  for FC1,
  - (b)  $(256, 256)$  for FC2,
  - (c)  $(512, 1)$  for FC3,
  - (d)  $(512, n_i)$  for FC4,
  - (e)  $(512, \dim(\mathbf{d}_i))$  for FC5,
  - (f)  $(\dim(\mathbf{p}(x)) + 1, \dim(\mathbf{p}(x)))$  for FC6,
  - (g)  $(\dim(\mathbf{p}(x)), \dim(\mathbf{p}(x)))$  for FC7 to FC13.

The number of modes in VGM is  $n_j = \{10, 20, 30\}$ . The learning rate decay factor and period are  $\psi = 0.97$ ,  $\xi = 2$  so there are almost no updates around 300 epochs and the model converges. All experiments were conducted in the following software and hardware environments: UBUNTU 18.04 LTS, PYTHON 3.6.6, NUMPY 1.18.5, SCIPY 1.5, MATPLOTLIB 3.3.1, PYTORCH 1.2.0, CUDA 10.0, and NVIDIA Driver 417.22, i9 CPU, and NVIDIA RTX TITAN.

**4.1.5 Experimental Results.** In Tables 2 and 3, all likelihood estimation results are included. CLBN and PrivBN show fluctuating performance. CLBN and PrivBN are good in Ring and Asia, respectively while PrivBN shows poor performance in Grid, and Gridr. TVAE shows good performance for  $\Pr(\mathcal{F}|\mathcal{S})$  in many cases but relatively worse performance than others for  $\Pr(T_{\text{test}}|\mathcal{S}')$  in Grid and Insurance, which means mode collapse. At the same time, TVAE shows nice performance for Gridr. All in all, TVAE shows reasonable performance in these experiments.

Among many GAN models except OCT-GAN, TGAN and TableGAN show reasonable performance, and other GANs are inferior to them in many cases, e.g., -14.3 for TableGAN vs. -14.8 for TGAN vs. -18.1 for VEEGAN in Insurance with  $\Pr(T_{\text{test}}|\mathcal{S}')$ . However, all these models are significantly outperformed by our proposed OCT-GAN. In all cases, OCT-GAN is better than TGAN, the state-of-the-art GAN model.

## 4.2 Classification with Real Data

**4.2.1 Data.** We consider 5 real-world datasets for classification: Adult [37], Census [37], Covertype [9], Credit [20], Intrusion [7]. Adult consists of diverse demographic information in the U.S., extracted from the 1994 Census Survey, where we predict two classes of high ( $> \$50K$ ) and low ( $\leq \$50K$ ) income. Census is similar to Adult

**Table 1: #C, #B, and #M mean the number of continuous columns, binary columns and multi-class discrete columns, respectively. C and R in Task mean classification and regression, respectively.**

Name	Simulated Data			Name	Real Data			Task		
	#train/test	#C	#B		#M	#train/test	#C		#B	#M
Grid	10k/10k	2	0	0	Adult	23k/10k	6	2	7	C
Gridr	10k/10k	2	0	0	Census	200k/100k	7	3	31	C
Ring	10k/10k	2	0	0	Coverttype	481k/100k	10	44	1	C
Asia	10k/10k	0	8	0	Credit	264k/20k	29	1	0	C
Alarm	10k/10k	0	13	24	Intrusion	394k/100k	26	5	10	C
Child	10k/10k	0	8	12	News	31k/8k	45	14	0	R
Insurance	10k/10k	0	8	19						

**Table 2: Likelihood estimation with Gaussian mixture models. The best (resp. the second best) results are highlighted in bold-face (resp. with underline). Our OCT-GAN outperforms TGAN, the state-of-the-art GAN-based model.**

Method	Grid		Gridr		Ring	
	$\Pr(\mathcal{F} \mathcal{S})$	$\Pr(\mathcal{T}_{\text{test}} \mathcal{S}')$	$\Pr(\mathcal{F} \mathcal{S})$	$\Pr(\mathcal{T}_{\text{test}} \mathcal{S}')$	$\Pr(\mathcal{F} \mathcal{S})$	$\Pr(\mathcal{T}_{\text{test}} \mathcal{S}')$
$T_{\text{train}}$	-3.06	-3.06	-3.06	-3.07	-1.70	-1.70
CLBN	-3.68	-8.62	-3.76	-11.60	-1.75	<b>-1.70</b>
PrivBN	-4.33	-21.67	-3.98	-13.88	-1.82	-1.71
MedGAN	-10.04	-62.93	-9.45	-72.00	-2.32	-45.16
VEEGAN	-9.81	-4.79	-12.51	-4.94	-7.85	-2.92
TableGAN	-8.70	-4.99	-9.64	-4.70	-6.38	-2.66
TVAE	<b>-2.86</b>	-11.26	<b>-3.41</b>	<b>-3.20</b>	<b>-1.68</b>	-1.79
TGAN	-5.63	-3.69	-8.11	-4.31	-3.43	-2.19
OCT-GAN(fixed)	-3.48	-3.47	-4.66	-3.96	-2.39	-1.97
OCT-GAN(only_G)	-3.41	-3.49	-4.96	-4.03	-2.49	-1.97
OCT-GAN(only_D)	-3.71	-3.51	-4.85	-4.0	-2.48	-1.98
OCT-GAN	<u>-3.32</u>	<b>-3.46</b>	-4.90	-4.09	-2.43	-1.98

**Table 3: Likelihood estimation with Bayesian networks. Our OCT-GAN outperforms TGAN, the state-of-the-art GAN-based model.**

Method	Asia		Alarm		Child		Insurance	
	$\Pr(\mathcal{F} \mathcal{S})$	$\Pr(\mathcal{T}_{\text{test}} \mathcal{S}')$	$\Pr(\mathcal{F} \mathcal{S})$	$\Pr(\mathcal{T}_{\text{test}} \mathcal{S}')$	$\Pr(\mathcal{F} \mathcal{S})$	$\Pr(\mathcal{T}_{\text{test}} \mathcal{S}')$	$\Pr(\mathcal{F} \mathcal{S})$	$\Pr(\mathcal{T}_{\text{test}} \mathcal{S}')$
$T_{\text{train}}$	-2.23	-2.24	-10.3	-10.3	-12.0	-12.0	-12.8	-12.9
CLBN	-2.44	-2.27	-12.4	-11.2	-12.6	-12.3	-15.2	-13.9
PrivBN	-2.28	<b>-2.24</b>	-11.9	-10.9	-12.3	<b>-12.2</b>	-14.7	<b>-13.6</b>
MedGAN	-2.81	-2.59	-10.9	-14.2	-14.2	-15.4	-16.4	-16.4
VEEGAN	-8.11	-4.63	-17.7	-14.9	-17.6	-17.8	-18.2	-18.1
TableGAN	-3.64	-2.77	-12.7	-11.5	-15.0	-13.3	-16.0	-14.3
TVAE	-2.31	-2.27	-11.2	<b>-10.7</b>	<u>-12.3</u>	<u>-12.3</u>	-14.7	-14.2
TGAN	-2.56	-2.31	-14.2	-12.6	-13.4	-12.7	-16.5	-14.8
OCT-GAN(fixed)	-2.51	-2.27	<b>-10.7</b>	-11.1	-12.5	-12.3	<b>-14.5</b>	-13.8
OCT-GAN(only_G)	-2.50	-2.27	-12.1	-11.6	<b>-12.1</b>	<b>-12.2</b>	-14.9	<u>-13.7</u>
OCT-GAN(only_D)	-2.35	-2.26	-11.9	-11.1	-12.5	<b>-12.2</b>	-14.8	<b>-13.6</b>
OCT-GAN	<b>-2.25</b>	<u>-2.27</u>	<u>-10.8</u>	<u>-10.9</u>	-12.6	<u>-12.3</u>	<u>-14.6</u>	-13.9

but it has different columns. Coverttype is to predict forest cover types from cartographic variables only and was collected from the Roosevelt National Forest of northern Colorado. Credit is for credit card fraud detection, collected from European cardholders in September 2013. Intrusion was used in the international Knowledge Discovery and Data Mining Competition and contains many network intrusion detection samples. Adult, Census, and Credit are binary classification datasets while others are for multi-class classification. We use  $T_{\text{train}}$  and  $T_{\text{test}}$  to denote training/testing data in each dataset. Their statistics are summarized in Table 1.

**4.2.2 Evaluation Methodology.** All those datasets provide well separated training/testing sets, and we use them for evaluation. We first train various generative models, including our OCT-GAN, with their training sets. With those trained models, we i) generate a fake table  $\mathcal{F}$ , ii) train Adaboost [51], DecisionTree [47], and Multi-layer

Perceptron (MLP) [8] with the fake table, and iii) test with  $T_{\text{test}}$ . We note that these base classifiers have many hyperparameters and we choose the best hyperparameter set for each classifier using the cross-validation method. We use F-1 (resp. Macro F-1) for the binary (resp. the multi-class) classification tasks.

**4.2.3 Experimental Results.** The classification results are summarized in Table 4. CLBN and PrivBN do not show any reasonable performance in these experiments even though their likelihood estimation experiments with simulated data are not bad. All their (Macro) F-1 scores fall into the category of worst-case performance, which proves potential intrinsic differences between likelihood estimation and classification — data synthesis with good likelihood estimation does not necessarily mean good classification.

**Table 4: Classification/regression with real data. ‘N/A’ means severe mode collapse.**

Method	Adult		Census	Credit	Cover.	Intru.	News
	F1	F1	F1	Macro	Macro	Macro	R <sup>2</sup>
T <sub>train</sub>	0.669	0.494	0.720	0.652	0.862	0.14	
CLBN	0.334	0.310	0.409	0.319	0.384	-6.28	
PrivBN	0.414	0.212	0.185	0.270	0.384	-4.49	
MedGAN	0.375	N/A	N/A	0.093	0.299	-8.80	
VEEGAN	0.235	0.094	N/A	0.082	0.261	-6.5e6	
TableGAN	0.492	0.358	0.182	N/A	N/A	-3.09	
TVAE	0.626	0.377	0.098	0.433	0.511	-0.20	
TGAN	0.601	0.391	0.672	0.324	0.528	-0.43	
OCT-GAN(fixed)	0.632	0.370	0.620	0.405	0.453	0.06	
OCT-GAN(only_G)	0.591	0.247	0.660	0.358	<b>0.552</b>	-4.35	
OCT-GAN(only_D)	0.631	<b>0.436</b>	0.689	0.364	0.454	-0.17	
OCT-GAN	<b>0.635</b>	<b>0.402</b>	<b>0.695</b>	<b>0.438</b>	<b>0.532</b>	<b>0.08</b>	

**Table 5: Clustering with real data (Silhouette score)**

Method	Adult		Census		Credit		Cover.	Intru.		
	T <sub>train</sub>	T <sub>test</sub>	T <sub>train</sub>	T <sub>test</sub>	T <sub>train</sub>	T <sub>test</sub>	T <sub>train</sub>	T <sub>test</sub>		
T <sub>train</sub>	0.61	0.61	0.41	0.39	0.40	0.40	0.16	0.15	0.87	0.86
TGAN	0.38	0.60	0.22	0.32	0.40	0.36	0.12	0.11	0.50	0.85
OCT-GAN(fixed)	0.54	0.60	<b>0.53</b>	0.41	0.37	0.53	0.13	0.11	<b>0.59</b>	0.71
OCT-GAN(only_G)	0.13	0.53	0.29	0.32	<b>0.42</b>	0.14	<b>0.16</b>	0.09	0.34	0.85
OCT-GAN(only_D)	0.57	0.62	0.25	0.32	0.36	<b>0.54</b>	0.08	<b>0.15</b>	0.27	0.67
OCT-GAN	<b>0.62</b>	<b>0.62</b>	0.49	<b>0.41</b>	0.34	<b>0.54</b>	0.12	0.10	0.45	<b>0.86</b>

TVAE shows reasonable scores in many cases. In Credit, however, its score is unreasonably low. This also corroborates the intrinsic difference between likelihood estimation and classification.

Many GAN models except TGAN and OCT-GAN show low scores in many cases, e.g., an F-1 score of 0.094 by VEEGAN in Census. Due to severe mode collapse in  $\mathcal{F}$ , we could not properly train classifiers in some cases and their F-1 scores are marked with ‘N/A’. However, our proposed OCT-GANs, including its variations, significantly outperform all other methods in all datasets.

### 4.3 Regression with Real Data

**4.3.1 Data.** We use News [26] in this experiment, which contains many features extracted from online news articles to predict the number of shares in social networks, e.g., tweets, retweets, and so forth. Therefore, this dataset is good to show the usefulness of our method in web-based applications.

**4.3.2 Evaluation Methodology.** We follow steps similar to the steps in the classification experiment. We use Linear Regression and MLP as base regression models and use R<sup>2</sup> as an evaluation metric [8].

**4.3.3 Experimental Results.** As shown in Table 4, all methods except OCT-GAN show unreasonable accuracy. The original model, trained with T<sub>train</sub>, shows an R<sup>2</sup> score of 0.14 and our OCT-GAN shows a score close to it. Only OCT-GAN and the original model, marked with T<sub>train</sub>, show positive scores.

### 4.4 Clustering with Real Data

**4.4.1 Data & Evaluation Methodology.** We use the 5 classification datasets. With  $K = \{|C|, 2|C|, 3|C|\}$ , where  $C$  is a set of class labels, we run K-Means++ [5] for  $\mathcal{F}$ . We choose a value of  $K$  resulting in the highest Silhouette score [49] to find the best  $K$ . With the found centroids of  $\mathcal{F}$ , we calculate a Silhouette score of applying the

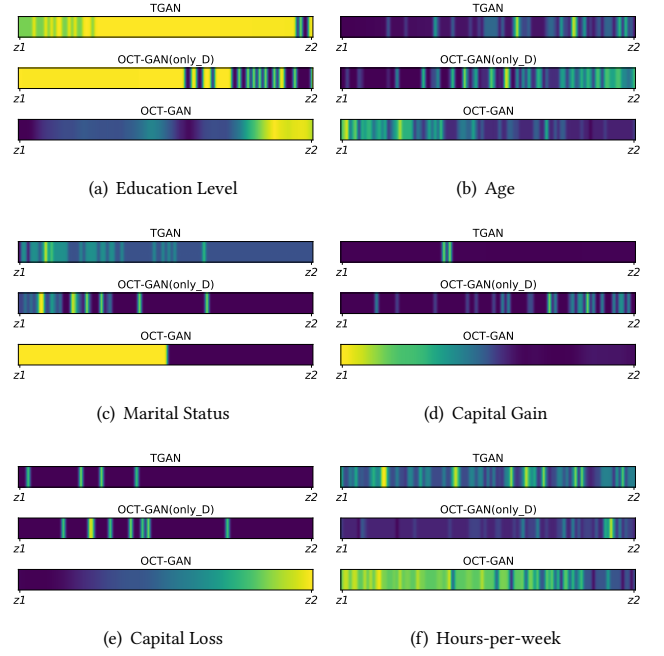


**Figure 6: Interpolation results for important columns in Adult – purple means the minimum value and yellow means the maximum value in each column. We use the models reported in Table 4 for this visualization.**

centroids to T<sub>train</sub> and T<sub>test</sub>. A low score for T<sub>train</sub> means potential mode collapse or incomplete synthesis.

**4.4.2 Experimental Results.** Table 5 summarizes the results by TGAN and OCT-GAN, the top-2 models for classification and regression, for space reasons. OCT-GAN outperforms TGAN in almost all cases.

### 4.5 Ablation Study

**4.5.1 Ablation Study Models.** To show the efficacy of key design points in our proposed model, we compare the full model with the following ablation study models:

- (1) In OCT-GAN(fixed), we do not train  $t_i$  but set it to  $t_i = \frac{i}{m}$ ,  $0 \leq i \leq m$ , i.e., evenly dividing the range  $[0, 1]$  into  $t_0 = 0, t_1 = \frac{1}{m}, \dots, t_m = 1$ .
- (2) In OCT-GAN(only\_G), we add an ODE layer only to the generator and the discriminator does not have it. We set  $D(x) = \text{FC5}(\text{leaky}(\text{FC4}(\text{leaky}(\text{FC3}(\mathbf{h}(0)))))$  in Eq. (8).
- (3) In OCT-GAN(only\_D), we add an ODE layer only to the discriminator and feed  $\mathbf{z} \oplus \mathbf{c}$  directly into the generator.

**4.5.2 Ablation Study Results.** In Tables 2 to 5, we also summarize the ablation study models’ performance. In Tables 2 and 3, those ablation study models surprisingly show better likelihood estimations than the full model, OCT-GAN, in several cases. However, we do not observe significant margins between the full model and the ablation study models (even when the ablation study models are better than the full model).



For the classification and regression experiments in Table 4, however, we can observe non-trivial differences among them in several cases. In `Adult`, for instance, `OCT-GAN(only_G)` shows a much lower score than other models. By this, we can know that in `Adult`, the ODE layer in the discriminator plays a key role. `OCT-GAN(fixed)` is almost as good as `OCT-GAN`, but learning intermediate time points further improves, i.e., 0.632 of `OCT-GAN(fixed)` vs. 0.635 of `OCT-GAN`. Therefore, it is crucial to use the full model, `OCT-GAN`, considering the high data utility in several datasets.

#### 4.6 Noisy Vector Interpolation

To further show the efficacy of the ODE-based transformation in the generator, we visualize several interpolation results in `Adult`. We select two noisy vectors  $z_1, z_2$  and interpolate many intermediate vectors by  $e z_1 + (1 - e) z_2$ , where  $0 < e < 1$ , to generate samples given a fixed random condition vector. In Fig. 6, we show those interpolation results in several columns of `Adult`. In our observation, `TGAN` and `OCT-GAN(only_D)` show similar interpolation patterns and `OCT-GAN` can interpolate in a smooth way.

### 5 DISCUSSIONS

One important discussing point is the difference between the likelihood fitness and the other machine learning experiments. In general, simple models, such as `PrivBN`, `TVAE`, and our ablation study models, show better likelihood estimations, and sophisticated models show better machine learning task scores. In real-world environments, however, we think that task-specific data utility is more important than likelihood. Therefore, `OCT-GAN` can benefit many applications.

However, the data utility of fake tabular data is not satisfactory yet in a couple of cases in our experiments, i.e., `Covertime` and `Intrusion` where all methods fail to show a score close to that of the original model marked with  $T_{\text{train}}$ , which shows the difficulty of data synthesis. They are all multi-class classification datasets. We think there is still a room to improve the quality (utility) of data synthesis for complicated machine learning tasks.

### 6 CONCLUSIONS

Tabular data synthesis is an important topic of web-based research. However, it is hard to synthesize tabular data due to its irregular data distribution and mode collapse. We presented a NODE-based conditional GAN, called `OCT-GAN`, carefully designed to address all those problems. Our method shows the best performance in many cases of the classification, regression, and clustering experiments. However, there is a room to improve for multi-class classification.

### ACKNOWLEDGMENTS

Jayoung Kim and Jinsung Jeon contributed equally to this research. Noseong Park is the corresponding author. This work was supported by the Institute of Information & Communications Technology Planning & Evaluation (IITP) grant funded by the Korea government (MSIT) (No. 2020-0-01361, Artificial Intelligence Graduate School Program (Yonsei University)).

### REFERENCES

[1] Jonas Adler and Sebastian Lunz. 2018. Banach Wasserstein GAN. In *NeurIPS*.

[2] A. Anand, K. Gorde, J. R. Antony Moniz, N. Park, T. Chakraborty, and B. Chu. 2018. Phishing URL Detection with Oversampling based on Text Generative Adversarial Networks. In *IEEE BigData*.

[3] Anthreas Antoniou, Amos Storkey, and Harrison Edwards. 2018. Data Augmentation Generative Adversarial Networks. In *ICLR*.

[4] Martin Arjovsky, Soumith Chintala, and Léon Bottou. 2017. Wasserstein Generative Adversarial Networks. In *ICML*.

[5] David Arthur and Sergei Vassilvitskii. 2007. K-Means++: The Advantages of Careful Seeding. In *SODA*.

[6] Laura Aviñó, Matteo Ruffini, and Ricard Gavaldà. 2018. Generating Synthetic but Plausible Healthcare Record Datasets. arXiv:1807.01514

[7] Stephen Bay, Dennis Kibler, Michael Pazzani, and Padhraic Smyth. 2002. The UCI KDD Archive of Large Data Sets for Data Mining Research and Experimentation. *ACM SIGKDD Explorations Newsletter* 2 (2002).

[8] Christopher M. Bishop. 2006. *Pattern Recognition and Machine Learning (Information Science and Statistics)*. Springer-Verlag.

[9] Jock A. Blackard and Denis J. Dean. 1999. Comparative accuracies of artificial neural networks and discriminant analysis in predicting forest cover types from cartographic variables. *Computers and Electronics in Agriculture* 24, 3 (1999), 131 – 151.

[10] Leon Bornemann, Tobias Bleifuß, Dmitri V. Kalashnikov, Felix Naumann, and Divesh Srivastava. 2020. Natural Key Discovery in Wikipedia Tables. In *The Web Conference*.

[11] Christopher Bowles, Liang Chen, Ricardo Guerrero, Paul Bentley, Roger Gunn, Alexander Hammers, David Alexander Dickie, Maria Valdés Hernández, Joanna Wardlaw, and Daniel Rueckert. 2018. GAN Augmentation: Augmenting Training Data using Generative Adversarial Networks. arXiv:1810.10863

[12] Matteo Cannavicchio, Denilson Barbosa, and Paolo Meriardo. 2018. Towards Annotating Relational Data on the Web with Language Models. In *The Web Conference*.

[13] Zhengping Che, Yu Cheng, Shuangfei Zhai, Zhaonan Sun, and Yan Liu. 2017. Boosting Deep Learning Risk Prediction with Generative Adversarial Networks for Electronic Health Records. (2017). arXiv:1709.01648

[14] Haipeng Chen, Sushil Jajodia, Jing Liu, Noseong Park, Vadim Sokolov, and VS Subrahmanian. 2019. FakeTables: Using GANs to Generate Functional Dependency Preserving Tables with Bounded Real Data. In *IJCAI*.

[15] Ricky T. Q. Chen, Yulia Rubanova, Jesse Bettencourt, and David K Duvenaud. 2018. Neural Ordinary Differential Equations. In *NeurIPS*.

[16] Edward Choi, Siddharth Biswal, A. Bradley Maline, Jon Duke, F. Walter Stewart, and Jimeng Sun. 2017. Generating Multi-label Discrete Electronic Health Records using Generative Adversarial Networks. (2017). arXiv:1703.06490

[17] Jaehoon Choi, Tae-Kyung Kim, and Changick Kim. 2019. Self-Ensembling With GAN-Based Data Augmentation for Domain Adaptation in Semantic Segmentation. In *ICCV*.

[18] C. Chow and C. Liu. 1968. Approximating discrete probability distributions with dependence trees. *IEEE Transactions on Information Theory* 14, 3 (1968), 462–467.

[19] Graham Cormode, Magda Procopiuc, Entong Shen, Divesh Srivastava, and Ting Yu. 2011. Differentially Private Spatial Decompositions. (2011). arXiv:1103.5170

[20] Andrea Dal Pozzolo, Olivier Caelen, Yann-Aël Le Borgne, Serge Waterschoot, and Gianluca Bontempi. 2014. Learned lessons in credit card fraud detection from a practitioner perspective. *Expert Systems with Applications* 41 (2014), 4915–4928.

[21] Talgat Daulbaev, Alexandr Katrutsa, Larisa Markeeva, Julia Gusak, Andrzej Cichocki, and Ivan Oseledets. 2020. Interpolated Adjoint Method for Neural ODEs. arXiv:2003.05271 (2020).

[22] J.R. Dormand and P.J. Prince. 1980. A family of embedded Runge-Kutta formulae. *J. Comput. Appl. Math.* 6, 1 (1980), 19 – 26.

[23] Fabio Henrique Kiyooiti dos Santos Tanaka and Claus Aranha. 2019. Data Augmentation Using GANs. arXiv:1904.09135

[24] Emilien Dupont, Arnaud Doucet, and Yee Whye Teh. 2019. Augmented Neural ODEs. In *NeurIPS*.

[25] Cristóbal Esteban, L. Stephanie Hyland, and Gunnar Rätsch. 2017. Real-valued (Medical) Time Series Generation with Recurrent Conditional GANs. arXiv:1706.02633

[26] Kelwin Fernandes. 2015. A Proactive Intelligent Decision Support System for Predicting the Popularity of Online News. In *EPLA*.

[27] Besnik Fetahu, Avishek Anand, and Maria Koutraki. 2019. TableNet: An Approach for Determining Fine-Grained Relations for Wikipedia Tables. In *The Web Conference*.

[28] Chris Finlay, Jörn-Henrik Jacobsen, Levon Nurbekyan, and Adam M Oberman. 2020. How to train your neural ODE: the world of Jacobian and kinetic regularization. In *ICML*.

[29] Ian Goodfellow, Jean Pouget-Abadie, Mehdi Mirza, Bing Xu, David Warde-Farley, Sherjil Ozair, Aaron Courville, and Yoshua Bengio. 2014. Generative Adversarial Nets. In *NeurIPS*.

[30] Saiping Guan, Xiaolong Jin, Yuanzhuo Wang, and Xueqi Cheng. 2019. Link Prediction on N-Ary Relational Data. In *The Web Conference*.

[31] Ishaan Gulrajani, Faruk Ahmed, Martin Arjovsky, Vincent Dumoulin, and Aaron Courville. 2017. Improved Training of Wasserstein GANs. In *NeurIPS*.

- [32] Braden Hancock, Hongrae Lee, and Cong Yu. 2019. Generating Titles for Web Tables. In *The Web Conference*.
- [33] Haque Ishfaq, Assaf Hoogi, and Daniel Rubin. 2018. TVAE: Triplet-Based Variational Autoencoder using Metric Learning. arXiv:1802.04403
- [34] P. Isola, J. Zhu, T. Zhou, and A. A. Efros. 2017. Image-to-Image Translation with Conditional Adversarial Networks. In *CVPR*.
- [35] James Jordon, Jinsung Yoon, and V. D. Mihaela Schaar. 2019. PATE-GAN: Generating Synthetic Data with Differential Privacy Guarantees. In *International Conference on Learning Representations*.
- [36] Tero Karras, Samuli Laine, and Timo Aila. 2019. A Style-Based Generator Architecture for Generative Adversarial Networks. In *CVPR*.
- [37] R Kohavi. 1996. Scaling up the accuracy of Naive-Bayes classifiers: A decision-tree hybrid. In *KDD*.
- [38] Stefano Massaroli, Michael Poli, Jinkyoo Park, Atsushi Yamashita, and Hajime Asama. 2020. Dissecting Neural ODEs. arXiv:2002.08071 [cs.LG]
- [39] Mehdi Mirza and Simon Osindero. 2014. Conditional Generative Adversarial Nets. arXiv:1411.1784
- [40] Konstantinos Nikolaidis, Stein Kristiansen, Vera Goebel, Thomas Plagemann, Knut Liestøl, and Mohan Kankanhalli. 2020. Augmenting Physiological Time Series Data: A Case Study for Sleep Apnea Detection. In *ECML PKDD*.
- [41] Baburao G Pachpatte. 1997. *Inequalities for differential and integral equations*. Elsevier.
- [42] Noseong Park, Mahmoud Mohammadi, Kshitij Gorde, Sushil Jajodia, Hongkyu Park, and Youngmin Kim. 2018. Data Synthesis based on Generative Adversarial Networks. (2018). arXiv:1806.03384
- [43] Shreyas Patel, Ashutosh Kakadiya, Maitrey Mehta, Raj Derasari, Rahul Patel, and Ratnik Gandhi. 2018. Correlated Discrete Data Generation Using Adversarial Training. (2018). arXiv:1804.00925
- [44] Neha Patki, Roy Wedge, and Kalyan Veeramachaneni. 2016. The Synthetic Data Vault. In *DSAA*.
- [45] Martin Pawelczyk, Klaus Broelemann, and Gjergji Kasneci. 2020. Learning Model-Agnostic Counterfactual Explanations for Tabular Data. In *The Web Conference*.
- [46] Alessio Quaglino, Marco Gallieri, Jonathan Masci, and Jan Koutník. 2020. SNODE: Spectral Discretization of Neural ODEs for System Identification. In *ICLR*.
- [47] J. R. Quinlan. 1986. Induction of Decision Trees. *Mach. Learn.* 1, 1 (1986), 81–106.
- [48] P. Jerome Reiter. 2005. Using CART to Generate Partially Synthetic, Public Use Microdata. *Journal of Official Statistics* 21 (01 2005), 441.
- [49] Peter J. Rousseeuw. 1987. Silhouettes: A graphical aid to the interpretation and validation of cluster analysis. *J. Comput. Appl. Math.* 20 (1987), 53 – 65.
- [50] Tim Salimans, Ian Goodfellow, Wojciech Zaremba, Vicki Cheung, Alec Radford, Xi Chen, and Xi Chen. 2016. Improved Techniques for Training GANs. In *NeurIPS*.
- [51] Robert E. Schapire. 1999. A Brief Introduction to Boosting. In *IJCAI*.
- [52] Marco Scutari. 2020. bnlearn - an R package for Bayesian network learning and inference. <http://www.bnlearn.com/bnrepository>.
- [53] solid IT gmbh. 2020. DB-Engines Ranking. <https://db-engines.com/en/ranking>.
- [54] Akash Srivastava, Lazar Valkov, Chris Russell, Michael U. Gutmann, and Charles Sutton. 2017. VEEGAN: Reducing Mode Collapse in GANs using Implicit Variational Learning. In *NeurIPS*.
- [55] Ngoc-Trung Tran, Viet-Hung Tran, Ngoc-Bao Nguyen, Trung-Kien Nguyen, and Ngai-Man Cheung. 2020. On Data Augmentation for GAN Training. arXiv:2006.05338
- [56] Ping Wang, Tian Shi, and Chandan K. Reddy. 2020. Text-to-SQL Generation for Question Answering on Electronic Medical Records. In *The Web Conference*.
- [57] Lei Xu, Maria Skoularidou, Alfredo Cuesta-Infante, and Kalyan Veeramachaneni. 2019. Modeling Tabular data using Conditional GAN. In *NeurIPS*.
- [58] Hanshu Yan, Jiawei Du, Vincent Y. F. Tan, and Jiashi Feng. 2020. On Robustness of Neural Ordinary Differential Equations. arXiv:1910.05513
- [59] Wenhao Yu, Wei Peng, Yu Shu, Qingkai Zeng, and Meng Jiang. 2020. Experimental Evidence Extraction System in Data Science with Hybrid Table Features and Ensemble Learning. In *The Web Conference*.
- [60] Jun Zhang, Graham Cormode, Cecilia M. Procopiuc, Divesh Srivastava, and Xiaokui Xiao. 2017. PrivBayes: Private Data Release via Bayesian Networks. *ACM Transactions on Database Systems* (2017).
- [61] Jun Zhang, Xiaokui Xiao, and Xing Xie. 2016. PrivTree: A Differentially Private Algorithm for Hierarchical Decompositions. (2016). arXiv:1601.03229
- [62] Shuo Zhang, Edgar Meij, Krisztian Balog, and Ridho Reinanda. 2020. Novel Entity Discovery from Web Tables. In *The Web Conference*.
- [63] Xingyao Zhang, Cao Xiao, Lucas M. Glass, and Jimeng Sun. 2020. DeepEnroll: Patient-Trial Matching with Deep Embedding and Entailment Prediction. In *The Web Conference*.
- [64] Juntang Zhuang, Nicha Dvornek, Xiaoxiao Li, Sekhar Tatikonda, Xenophon Papademetris, and James Duncan. 2020. Adaptive Checkpoint Adjoint Method for Gradient Estimation in Neural ODE. In *ICML*.